Robotica (2018) volume 36, pp. 1920–1942. © Cambridge University Press 2018
doi:10.1017/S0263574718000802

Robust position-based impedance control of lightweight single-link flexible robots interacting with the unknown environment via a fractional-order sliding mode controller

Ali Fayazi†, Naser Pariz†*, Ali Karimpour† and Seyed Hassan Hosseinnia†‡

†*Department of Electrical Engineering, Ferdowsi University of Mashhad, Mashhad, Iran*
‡*Department of Precision and Microsystems Engineering, Delft University of Technology, Delft, Netherlands*

(Accepted July 29, 2018. First published online: September 7, 2018)

SUMMARY
This paper presents a fractional-order sliding mode control scheme equipped with a disturbance observer for robust impedance control of a single-link flexible robot arm when it comes into contact with an unknown environment. In this research, the impedance control problem is studied for both unconstrained and constrained maneuvers. The proposed control strategy is robust with respect to the changes of the environment parameters (such as stiffness and damping coefficient), the unknown Coulomb friction disturbances, payload, and viscous friction variations. The proposed control scheme is also valid for both unconstrained and constrained motions. Our novel approach automatically switches from the free to the constrained motion mode using a simple algorithm of contact detection. In this regard, an impedance control scheme is proposed with the inner loop position control. This means that in the free motion, the applied force to the environment is zero and the reference trajectory for the inner loop position control is the desired trajectory. However, in the constrained motion the reference trajectory for the inner loop is determined by the desired impedance dynamics. Stability of the closed loop control system is proved by Lyapunov theory. Several numerical simulations are carried out to indicate the capability and the effectiveness of the proposed control scheme.

KEYWORDS: Robust impedance control; Fractional-order sliding mode control; Disturbance observer; Single-link flexible robots; Unknown environment.

1. Introduction

Over the past few decades, research on flexible manipulators has been developed since new robotics applications have arisen in different areas such as industrial robots applications. The tendency in these applications is to use the lightweight materials in the construction of manipulators in order to improve their performance, i.e., high speed, high precision, and high payload/weight ratio. In ref. [1], some of the applications of flexible manipulators have been reviewed—for example, robotic booms in the aerospace industry, where the lightweight of the manipulators are an essential requirement;[2] the control of large structures, such as boom cranes and fire rescue turntable-ladders, which are treated as flexible link robots;[3] motion control of robotic sensing antenna systems;[4,5] and minimally invasive surgery carried out with thin flexible instruments in which precise automatic manipulators are necessary.[6]

A very lightweight flexible robot system has several advantages over the traditional rigid robot manipulators. These advantages consist lower energy consumption, relatively smaller actuators, lower cost, higher maneuverability, better transportability, and higher payload-to-arm weight ratio.

* Corresponding author. E-mail: n-pariz@um.ac.ir

Moreover, the severity of collision with obstacles or human is reduced because of the flexibility of the arm. In spite of these advantageous features, its control is very difficult. One of these difficulties is the suppression of vibrations caused by structural flexibility and the other one arises from the complex model of the flexible manipulators.

In general, all of the aforementioned robotic tasks can be classified into two different categories: unconstrained and constrained motion. In the first case, the manipulator is driven in its workspace without contact with the environment (free motion of the manipulator). In the second case, the manipulator interacts with its environment. In this situation the environment continuously exerts a dynamics or kinematic constraint on the manipulator's motion.

Impedance control, compliance control, and hybrid position/force control are three main approaches, which are usually used to control flexible manipulators. Among those, impedance control has a universal feature that makes it more efficient in the compliant motions control. Therefore, it is widely used to control the end-effector of robot manipulators while interacting with an environment. The idea of impedance control was presented by Hogan for the first time.[7] In this method, neither the position nor the force is used for control, but a generalized impedance equation, which combines the position and force errors, is utilized. This equation is defined as the target impedance between the motion (position and orientation) and the interaction loads (forces and torques). Therefore, the impedance control system is reduced to a position control system during unconstrained maneuvers (free motion) and is performed as a force control system during constrained maneuvers.

Impedance control of the constrained robotic systems has been a well-known framework in the robot control in the past two decades. Nowadays, its importance becomes more tangible since robot applications are oriented toward assisting human. Some of these practical tasks are as follows: assembly, grinding, cutting, drilling, insertion, joining, contour following, scribing, drawing, and deburring that associate with an interaction between the flexible arm and environment.

Impedance control of the rigid manipulator has been extensively reviewed in the literature in the last two decades.[8–15] Many researchers have investigated position control, force control, and hybrid position/force control. However, the robust impedance control of the flexible manipulator has been rarely addressed in the literature.

In recent decades, various control strategies have been proposed on the subject of flexible manipulators interacting with the environment.[16–22] The main goal of these works is to cancel the vibrations caused by structural flexibility. Some of these control strategies can be found in refs. [23–26]. In refs. [24] and [25], a fractional-order active vibration suppression technique is used to control a flexible structure. In this work, a piezoelectric actuator is attached externally to the flexible structure to suppress the unwanted vibrations. In ref. [18], two nested control loop are proposed based on sliding mode control (SMC) for the position control of a very lightweight single-link flexible robot, which is robust to payload changes and motor friction. Each of these control loops is controlled by an independent sliding mode controller. In ref. [16], a position control strategy, consisting of two inner and outer loops, is proposed for two degrees of freedom flexible link. The inner loop is used to control the position of two servo-motors, and the outer-loop is used to cancel the tip vibration. In ref. [19], force control of a very lightweight single-link flexible manipulator based on coupling torque feedback is studied. The main objective of this work is regulation of the contact force that exerted by a very lightweight single-link flexible manipulator when it comes into contact with a motionless environment. Force control problem is studied for both free and constrained motions of the flexible manipulator, and a collision detection algorithm is also described. A modified proportional-integral-derivative (PID) controller is used to realize the aforementioned objective. In ref. [20], the modeling and the impedance control of a single-link flexible arm is presented for both constrained and unconstrained maneuvers.

In most of the reported articles related to the control of a single-link flexible arm interacting with the environment,[19,20] two separate controllers are suggested to control the system for two different operating modes (free and constrained motions). Therefore, two different dynamic models are required for these operating modes. Moreover, a collision detection algorithm is also required for switching the controller from the unconstrained to the constrained motion mode. In addition, the parameters of the system model such as stiffness and damping coefficient have to be known. In our novel approach, we proposed only one unified model for a single-link flexible arm, which is valid for both unconstrained and constrained motions. Moreover, the dynamics parameters of environment are completely unknown. In order to design the controller, we use the information

https://doi.org/10.1017/S0263574718000802 Published online by Cambridge University Press

of a motionless hypothetical object with pre-defined dynamics parameters. The parameters of the hypothetical environment can be different from the real environment.

In this paper, a robust impedance control strategy is presented for a very lightweight single-link flexible arm interacting with the unknown environment using the SMC theory. Fractional-order control (FOC) has been shown to be a promising tool in the field of control, mechatronics, and biological systems.[4,5,27–40] Therefore, the combination of the FOC and the SMC is proposed in order to improve the performance of the controller. The main contribution of this paper is that only one model of a single-link flexible arm is offered for both constrained and free motion modes. As a consequence of the unified model of the flexible link, we proposed a unified controller based on the impedance control concept equipped with a disturbance observer, which is valid for both free and constrained motions. Thus, without needing a separate algorithm to detect collision between the link and the environment, the controller switches automatically from the free to the constrained motion mode. Therefore, the proposed unified controller is valid for both free and constrained motions. In general, the collision point between the flexible arm and unknown environment could occur at any point on the robot. However, in many applications, especially industrial manipulator, the collision point is often at the end-effector. In this regard, the position based on impedance control system is proposed with force tracking. This means that in the free motion, the applied force to the environment is zero and the reference trajectory for the inner loop position control is the desired trajectory. In the constrained motion, the reference trajectory for the inner loop position is determined by the desired impedance model. Assuming the performance of the inner loop position controller is accurate and the dynamics and the geometry properties of the environment are known, the stiffness gain of the desired impedance could be selected so that the contact force is regulated to the desired value. Therefore, the precise design of the inner loop position controller is the important part of this work in the impedance control.

This paper is organized as follows. In Section 2, the modeling of the single-link flexible arm is addressed. In Section 3, the robust impedance control strategy is discussed based on the conventional SMC and the fractional-order sliding mode control (FSMC). The stability analysis of closed-loop control system and the definitions of the performance criteria are presented in Sections 4 and 5, respectively. In Section 6, the simulation results is provided to illustrate the effectiveness of the proposed control scheme. Finally, the conclusions are given in Section 7.

2. Modeling of Lightweight Single-Link Flexible Arm

Modeling the dynamics of a single-link flexible arm is comprised of two parts: the dynamics of a rigid part, also entitled as actuator, including a DC motor with a reduction gear operated by a current servo-amplifier, which produces the spatial movement of the structure; and the dynamics of a flexible part, which presents distributed elasticity along the whole structure. In the following, the DC motor and single-link flexible manipulator dynamics are described, respectively.

2.1. Motor dynamics

In this work, a DC motor with a reduction gear is used as a common electromechanical actuator, in many control systems in order to drive the single-link flexible slewing beam. This actuator is operated by a current servo-amplifier. The current servo-amplifier controls the input current to the motor, which is proportional to the voltage supplied to the servo-amplifier by the computer. The block diagram of the actuator (servo-amplifier + motor + gear) is shown in Fig. 1, whose equations are given as follows:[19]

$$Motor : \Gamma_m = k_m i = J\ddot{\theta}_m + v\dot{\theta}_m + \Gamma_{coul} + \Gamma_{coup} \tag{1}$$

$$Servo\text{-}amplifier : i = k_a V \tag{2}$$

$$Gear : \theta_m = \theta_l n;\ \Gamma_{coup} = \frac{\Gamma_l}{n} \tag{3}$$

where $\hat{\Gamma}_m$ is the motor torque, k_m is the electromechanical constant of the motor, i is the current supplied to the motor by the servo-amplifier, J is the motor inertia, v is the viscous friction of the motor, θ_m is the motor angle, θ_l is the motor angle in the gear outlet (load angle), Γ_{coul} is the Coulomb friction torque, Γ_l is the coupling torque between the flexible slewing link and the motor shaft (load angle), V is the voltage supplied to the servo-amplifier generated by the computer, k_a is the

https://doi.org/10.1017/S0263574718000802 Published online by Cambridge University Press

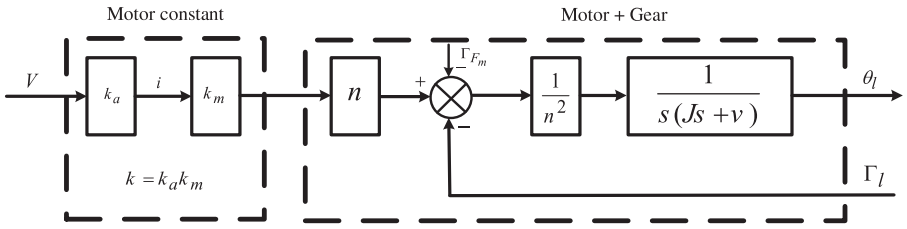

Fig. 1. Block diagram of the actuator.

servo-amplifier gain, and n is the reduction ratio of the gear. Therefore, by combining Eqs. (1)–(3), the complete actuator system dynamics is obtained by the following equation:

$$knV = Jn^2\ddot{\theta}_l + vn^2\dot{\theta}_l + \Gamma_{F_m} + \Gamma_l \tag{4}$$

where $k = k_m k_a$ and $\Gamma_{F_m} = n\Gamma_{Coul}$. The coulomb friction is considered as a perturbation that affects the system dynamics. This perturbation depends on the sign of the motor angular velocity. Therefore, the model of the coulomb friction torque can be defined by the following equation:

$$\Gamma_{coul} = \begin{cases} \Gamma_c \cdot \text{sign}(\dot{\theta}_m) & \dot{\theta}_m \neq 0 \\ \text{sign}(V) \cdot \min(k\,|V|\,, \Gamma_c) & \dot{\theta}_m = 0 \end{cases} \tag{5}$$

where Γ_c is a constant value, which is different for each motor and represents the static friction value that the motor torque must exceed to begin the movement, also called the Coulomb friction coefficient. The first case shows the Coulomb friction torque when the motor is moving, and the second case shows the same torque when the motor is stopped.

2.2. Link dynamics: Constrained movement

There are several methods that can be used to reduce the link dynamics, such as the lumped parameter model in which the finite element method can be utilized to discretize the spatial,[41] or a lumped-mass model,[42] or the truncation of a distributed parameter model.[43] In this work, the lumped-mass model as described in ref. [44] is used to obtain the reduced flexible link dynamics with tip mass. Figure 2 depicts the single-link flexible arm in constrained motion mode, which it comes into contact with unknown environment at the end-effector. Next, the following assumptions are considered:

- Assumption 1: All the mass concentrated at the tip position.
- Assumption 2: The tip mass is considered to freely rotate, and therefore, no rotational inertia from it affects the link dynamics.
- Assumption 3: There is only one collision point.
- Assumption 4: The single-link flexible manipulator rotates in a horizontal plane (the z axis perpendicular to the plane of the figure).
- Assumption 5: The deformations in the structure is very small, which allows to assume geometrical linearity, i.e., $\sin(x) \approx x$, $\tan(x) \approx x$.
- Assumption 6: The structure oscillates with the fundamental mode of vibration without the higher modal densities being excited, since it is assumed that the mass of the load is much larger than the arm's weight.

Assumption 6 allows us to neglect the other modes of vibration in order to obtain a simple model for the controller design. The nonlinear dynamics model for the tip angle can be described by the following equations:[44]

$$\begin{aligned} ml^2\ddot{\theta}_t &= K_1\,(\theta_l - \theta_t) + K_3(\theta_l - \theta_t)^3 - 2\xi l\,\cos\left(\alpha(\theta_t - \theta_l)\right)\sqrt{mK_1}\dot{\theta}_t - mgl\cos(\theta_t) + F_c l, \\ F_c &= -F_e \end{aligned} \tag{6}$$

$$\Gamma_l = K_1\,(\theta_l - \theta_t) + K_3(\theta_l - \theta_t)^3 \tag{7}$$

where m is the tip mass, l is the length of the arm, ξ is a friction coefficient, and g is referred to as the acceleration of gravity. F_c is the contact force, F_e is the interaction force applied on the object, θ_t is

https://doi.org/10.1017/S0263574718000802 Published online by Cambridge University Press

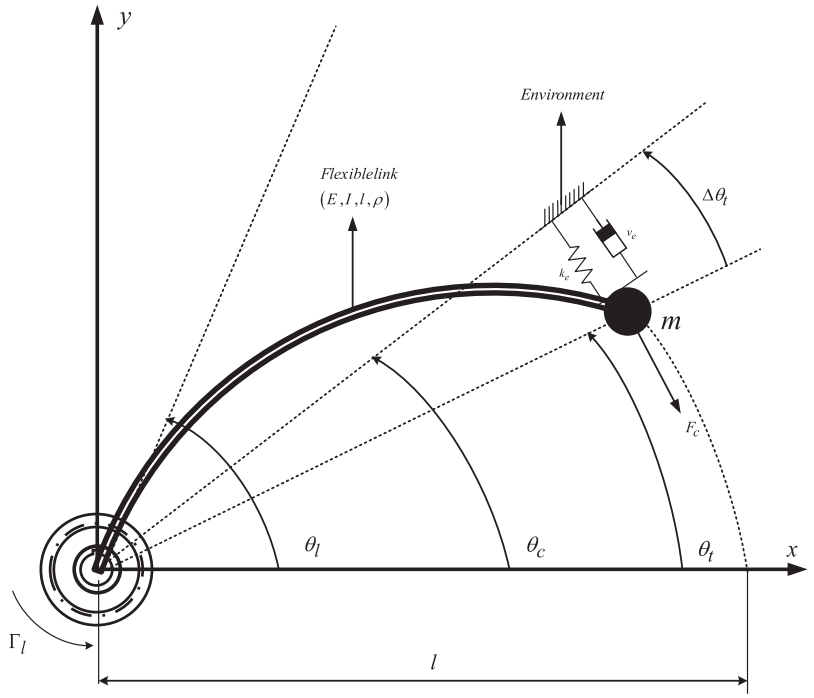

Fig. 2. Single-link flexible arm.

the angular position of the tip mass, α is a parameter to be adjusted, and K_1 and K_3 are the rotational stiffness coefficients of the arm that are considered constant throughout the whole flexible structure, as described in ref. [44].

In the following, it is assumed that the contact force is defined by its normal component. Therefore, the tangential component is ignored. It is also assumed that the normal component of the contact force is along the y-axis. Moreover, there is only one collision point between the tip mass and the unknown environment, which is occurring at the end-effector. Furthermore, it is assumed that the mechanical impedance of the unknown environment is represented by the following equation:

$$F_e = k_e(y - y_c) + v_e \frac{d(y - y_c)}{dt} \tag{8}$$

where y_c is the static equilibrium point of the object. Substituting $y = l\theta_t$ and $y_c = l\theta_c$ into (8) results

$$F_e = k_e l(\theta_t - \theta_c) + v_e l \frac{d(\theta_t - \theta_c)}{dt} \tag{9}$$

where k_e and v_e are the stiffness and damping characteristics of the unknown environment, and θ_c is the initial contact angle of the tip mass with the object. Since y_c is a fixed point in the plane, $\frac{d(\theta_c)}{dt} = 0$, and Eq. (9) is transformed as follows:

$$F_e = k_e l(\theta_t - \theta_c) + v_e l \frac{d(\theta_t)}{dt} \tag{10}$$

Therefore, the environment impedance is modeled by the well-known spring-damper system. Substituting (10) in (6) yields

$$\Gamma_l = ml^2\ddot{\theta}_t + 2\xi l \cos(\alpha(\theta_t - \theta_l))\sqrt{mK_1}\dot{\theta}_t + mgl\cos(\theta_t) + k_e l^2(\theta_t - \theta_c) + v_e l^2 \tfrac{d(\theta_t)}{dt} \tag{11}$$

https://doi.org/10.1017/S0263574718000802 Published online by Cambridge University Press

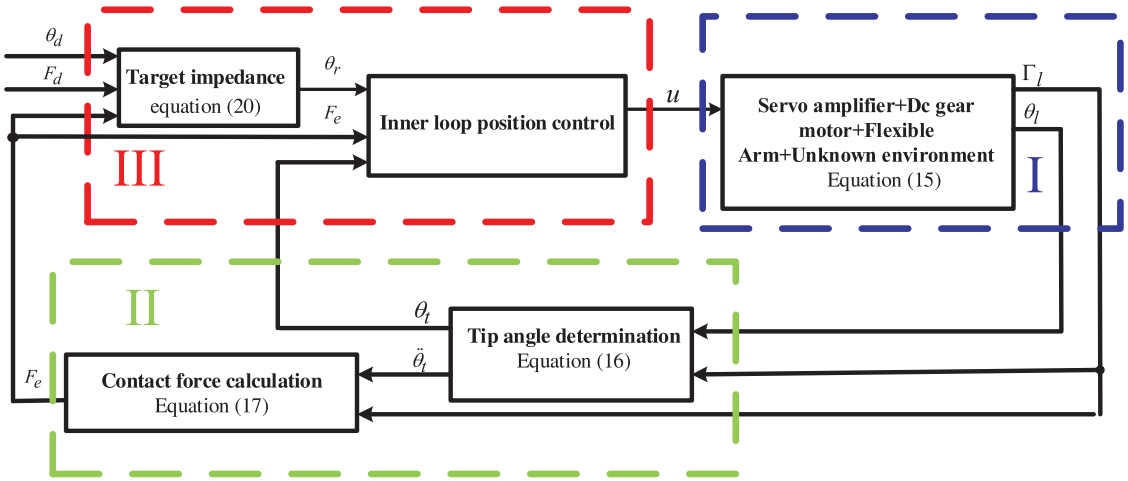

Fig. 3. Robust impedance control scheme based on the inner loop position control with force tracking.

If we make a change of angular coordinates in which we denote $\Delta\theta_t = \theta_t - \theta_c$ and $\Delta\theta_l = \theta_l - \theta_c$, then expressions (11), (10), and (7) become as follows:

$$\Gamma_l = ml^2\Delta\ddot{\theta}_t + 2\xi l\,\cos\left(\alpha(\Delta\theta_t - \Delta\theta_l)\right)\sqrt{mK_1}\Delta\dot{\theta}_t + mgl\cos\left(\Delta\theta_t\right) + k_e l^2\Delta\theta_t + v_e l^2\Delta\dot{\theta}_t \tag{12}$$

$$F_e = k_e l\Delta\theta_t + v_e l\frac{d(\Delta\theta_t)}{dt} \tag{13}$$

$$\begin{aligned}\Gamma_l &= K_1\left(\theta_l - \theta_c - \theta_t + \theta_c\right) + K_3(\theta_l - \theta_c - \theta_t + \theta_c)^3 \\ &= K_1\left(\Delta\theta_l - \Delta\theta_t\right) + K_3(\Delta\theta_l - \Delta\theta_t)^3\end{aligned} \tag{14}$$

Choosing $x_1 = \Delta\theta_t$ and $x_2 = \Delta\dot{\theta}_t$ as state variables and u $= \Delta\theta_l$ as input, $y_1 = F_e$ and $y_2 = \Gamma_l$ as outputs. The nonlinear model for the tip angle in the state-space representation can be achieved by the following equations:

$$\begin{cases}\dot{x}_1 = x_2 \\ \dot{x}_2 = \frac{K_1}{ml^2}(u - x_1) + \frac{K_3}{ml^2}(u - x_1)^3 - \frac{k_e}{m}x_1 - \frac{v_e}{\mathrm{m}}x_2 - \frac{2\xi}{ml}\cos\left(\alpha(x_1 - u)\right)\sqrt{mK_1}x_2 - \frac{g}{l}\cos\left(x_1\right) \\ \mathrm{y}_1 = k_e l x_1 + v_e l x_2 \\ \mathrm{y}_2 = K_1(u - x_1) + K_3(u - x_1)^3\end{cases} \tag{15}$$

3. Controller Design

In this section, a unified control system is designed for the robust impedance control of the single-link flexible arm, which is valid for both free and constrained motions. Figure 3 details the control scheme in which block I demonstrates the nonlinear plant analyzed in the preceding section for constrained motions (servo-amplifier + DC gear motor + arm + unknown environment), block II determines the position of the tip angle and calculates the contact force that is exerted to the environment, and block III represents the robust impedance control based on the inner loop position control with force tracking which the inner loop position control is a sliding mode controller. The detail of the block I is shown in Fig. 4. As can be seen from Fig. 4, a simple algorithm based on the angular position of environment is used to detect the collision for modeling the flexible link in the free and constrained motion mode.

Before we design the controller, it should be considered that the model must be valid for both constrained and free movements. In other words, only one dynamics model must be developed for the single-link flexible arm. To this respect, we utilize the nonlinear dynamics model (15) in constrained motion mode, which is valid for the free motion mode. The only difference of constrained and unconstrained maneuvers is taking into consideration of the contact force that is applied to the

https://doi.org/10.1017/S0263574718000802 Published online by Cambridge University Press

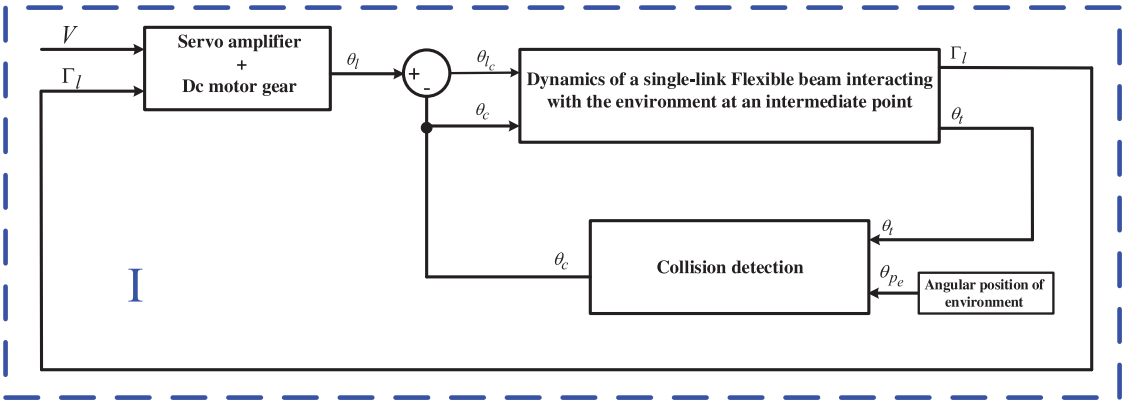

Fig. 4. Dynamics model of actuator, flexible link, and environment.

environment. The free motion can be considered as the constrained motion mode, assuming that the end-effector in the free motion mode with zero initial contact angle had hit the object with zero impedance.

After determining the unified model that is able to represent the dynamics characteristics of the flexible link in both constrained and free motions mode, the unified controller is designed with only one parameter set, which is satisfying the control requirements. As mentioned in Section 1, in the free motion mode, the applied force to the environment is zero and the reference trajectory for the inner loop position control is the desired trajectory (θ_d). In the constrained motion, the reference trajectory for the inner loop position is determined by the desired impedance dynamics, which is generated by target impedance block in Fig. 3 (θ_r). Assuming the inner loop position controller is accurate and the dynamics and the geometry of the environment are known, the stiffness gain of the desired impedance could be selected so that the contact force is regulated to the desired value. Therefore, the precise design of the inner loop position controller is the main objective of this work for the robust impedance control. In the following, the function of the blocks II and III will be explained.

3.1. Determination of the tip angle position and calculation of the contact force (block II)

The difference between the flexible link and the rigid link (with stiff actuator) is that the motor angle is not equal to the other points angle of the link. In other words, each point on the flexible link has some deflection in comparison to the rigid one. Despite this deflection, the tip angle someway must be regulated to the reference trajectory by the controller. Therefore, to obtain an accurate position control, it is necessary that the effect of the link flexibility is eliminated. In the impedance control, for calculating the desired impedance gain to regulate the contact force to a desired value, the collision point angle, dynamics parameters of the object, and measurement of the contact force are needed. Besides, the only measurable values are the load torque (Γ_l) and the load angular position (θ_l). Therefore, the information of the collision point angle and the contact force should be achieved by using these two values and the governing dynamical equations. By discarding the higher order term from (7) due to the small deflection of the beam, the tip angle can be approximated as follows:

$$\theta_t \triangleq \theta_l - \frac{\Gamma_l}{K_1} \tag{16}$$

The interaction force applied on the object is also obtained by substituting (7) into (6):

$$F_e = \frac{1}{l}\left(\Gamma_l - ml\ddot{\theta}_t - 2\xi l\ \cos\left(\alpha(\theta_t - \theta_l)\right)\sqrt{mK_1}\dot{\theta}_t - mg\text{lcos}\left(\theta_t\right)\right) \tag{17}$$

https://doi.org/10.1017/S0263574718000802 Published online by Cambridge University Press

If the stiffness and damping parameters are known, using Eq. (13) the initial contact angle of the tip mass with the object (θ_c) can be easily determined according to the following equation:

$$\theta_c = \theta_t + \frac{\nu_e}{k_e}\dot{\theta}_t - \frac{F_e}{(k_e l)} \tag{18}$$

This equation can be used to calculate the initial contact angle of the tip mass with the object when the dynamics parameters of the environment (k_e and ν_e) are known. However, in this study, these parameters are assumed to be unknown. Therefore, Eq. (18) should be used in another way by assuming that the link comes into contact with a motionless hypothetical object with known stiffness and damping coefficients (k_e^* and v_e^*). In the next section, this information of the hypothetical object must be used to calculate the desired impedance gain to regulate the interaction force applied on the object to the desired value. Thus, the position of the motionless hypothetical object (θ_c^*) can be easily obtained as follows:

$$\theta_c^* = \theta_t + \frac{v_e^*}{k_e^*}\dot{\theta}_t - \frac{F_e}{\left(k_e^* l\right)} \tag{19}$$

3.2. Robust impedance control scheme based on the inner loop position control with force tracking (block III)

3.2.1. Robust impedance control scheme. The objective of impedance control is to create a desired dynamics behavior between the interaction force exerted on the object and displacement affected by the object deformation. For achieving the desired impedance behavior the position and contact force must be regulated. A target impedance equation, which combines the position and the interaction force is, usually, of the second-order linear system and is given by:

$$F_e = k_m\left(\ddot{\theta}_d - \ddot{\theta}_r\right) + k_d\left(\dot{\theta}_d - \dot{\theta}_r\right) + k_p\left(\theta_d - \theta_r\right) \tag{20}$$

where θ_d and θ_r represent the desired angle and the reference angle for the inner loop position controller, respectively. F_e is the interaction force applied on the object, which is obtained from (9). Moreover, k_m, k_d, and k_p are target parameters for the desired impedance. In the steady state, by assuming the accurate inner loop position control and regulating the contact force to a desired value, Eqs. (20) and (9) are re-written as follows:

$$F_d = k_p^*\left(\theta_d - \theta_t\right) \tag{21}$$

$$F_d = k_e^* l\left(\theta_t - \theta_c^*\right) \tag{22}$$

In Eq. (21), k_p^* is the impedance gain corresponding to the information of the motionless hypothetical object to regulate the interaction force to the desired value (F_d). Therefore, by using Eqs. (21) and (22), the impedance stiffness coefficient could be selected such that the interaction force applied on the object is regulated to the desired value as the following equation:

$$k_p^* = \frac{F_d k_e^* l}{k_e^* l\left(\theta_d - \theta_c^*\right) - F_d} \tag{23}$$

3.2.2. Inner loop position control. As aforementioned, the main part of the impedance control design in this work is related to the design of the inner loop position control. Eliminating the deflection caused by the link flexibility is the significant challenge of the position control in the flexible link. To solve this challenge, one may consider the flexible link as a rigid one by assuming that the deflection of the flexibility is caused by a input disturbance. In this research, first, the sliding mode controller is used for the inner position control loop. A fractional-order sliding mode controller is, then, applied in order to improve the proposed controller performance. In order to eliminate the effect of deflection, the proposed sliding mode controller is equipped with a disturbance observer. Figure 5 details the inner loop position control block based on the fractional-order sliding mode controller.

https://doi.org/10.1017/S0263574718000802 Published online by Cambridge University Press

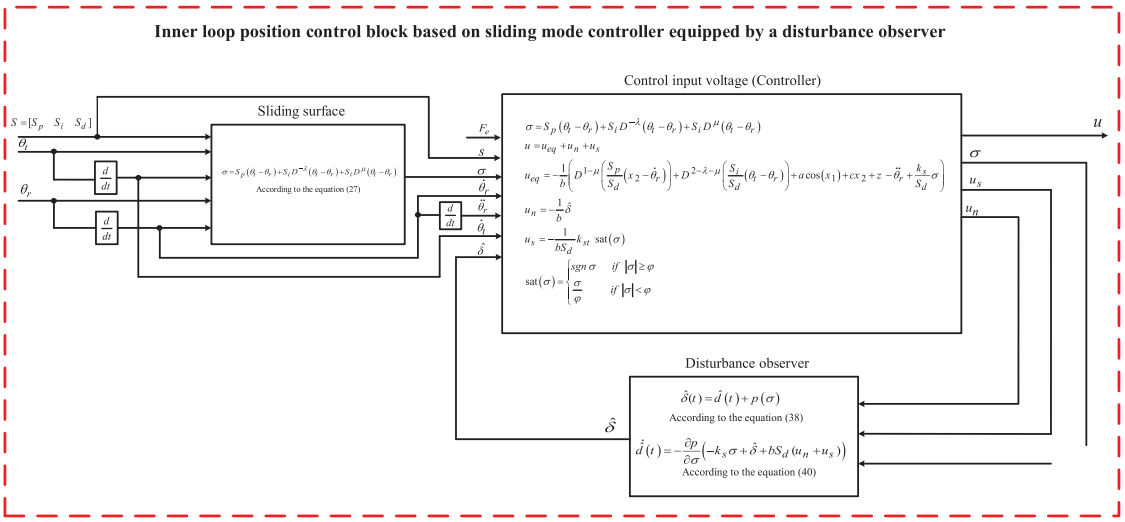

Fig. 5. Inner loop position control block based on a fractional-order sliding mode controller equipped with a disturbance observer.

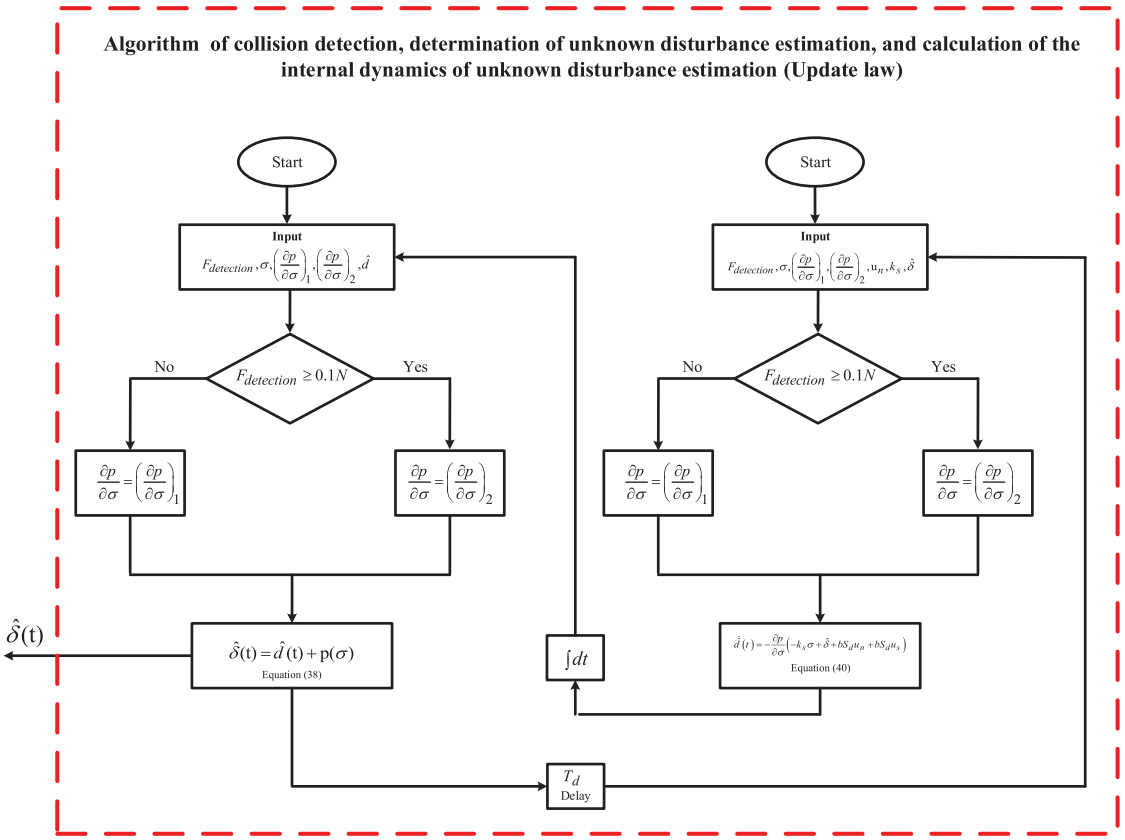

Fig. 6. The details of disturbance observer in which a simple algorithm is used to detect the collision.

The details of the disturbance observer are shown in Fig. 6. As can be seen in Fig. 6, a simple algorithm is used to detect the collision based on the measurement of contact force and in comparison with a specific threshold value being 0.1 N. Formulation of disturbance observer will be discussed in detail in Section 3.2.5.

In the next subsection, the fractional-order sliding mode controller equipped with a disturbance observer is described.

https://doi.org/10.1017/S0263574718000802 Published online by Cambridge University Press

3.2.3. Fractional-order sliding mode controller equipped with a disturbance observer. The interaction force applied on the environment is given by Eq. (17). Substituting (17) into (12) results

$$\Gamma_l = ml^2\Delta\ddot{\theta}_t + 2\xi l\,\cos\left(\alpha(\Delta\theta_t - \Delta\theta_l)\right)\sqrt{mK_1}\Delta\dot{\theta}_t + mg\mathrm{lcos}\left(\Delta\theta_t\right) + F_e l \tag{24}$$

Equation (4), which is related to the dynamics of actuator system, can be rewritten as follows:

$$knV = Jn^2\Delta\ddot{\theta}_l + vn^2\Delta\dot{\theta}_l + \Gamma_{F_m} + \Gamma_l \tag{25}$$

In this study, the main idea in the position control of the flexible link is based on this assumption that the deflection of the beam tip can be considered as a disturbance in the control input. Thus, according to this hypothesis, the tip angular position of the beam (θ_t) is considered as equal as the motor angular position (θ_l). Instead, the source of the beam deflection is considered in the voltage input. Therefore, the governing dynamical equation of the flexible link with the motor dynamics becomes a second-order equation that in the state–space representation can be expressed as follows:

$$\begin{cases} \dot{x}_1(t) = x_2(t) \\ \dot{x}_2(t) = a\,\cos\left(x_1\right) + cx_2 + b\left(u(t) + V_d(\mathrm{t})\right) + z + \Gamma^d_{F_m} \end{cases} \tag{26}$$

where $x_1(t) = \Delta\theta_t(t)$, $x_2(t) = \Delta\dot{\theta}_t(t)$, $a = -\frac{mgl}{Jn^2+ml^2}$, $c = -\frac{vn^2+2\xi l\sqrt{mK_1}}{Jn^2+ml^2}$, $b = \frac{Kn}{Jn^2+ml^2}$, and $\mathrm{z} = -\frac{F_e l}{Jn^2+ml^2}$. $\Gamma^d_{F_m}$ is the Coulomb friction disturbances, and $u(t)$ and $V_d(\mathrm{t})$ represent the control signal and the input disturbance, respectively. In the SMC theory, an appropriate sliding surface is selected and the control input is, then, designed to ensure the SMC finite time reaching condition is satisfied. This makes the system robust against uncertainties such as parameter variations, frictions, and disturbances. In the following, a generalized fractional-order surface ($PI^{\lambda}D^{\mu}$) is used for SMC. It is a general surface that includes three other known surfaces, i.e., PID ($\lambda = 1$, $\mu = 1$), PD ($\lambda = 0$, $\mu = 1$ and $S_i = 0$), and a fractional-order surface sliding mode controller PD^{μ} ($S_i = 0$).[45]

3.2.4. Generalized fractional-order $PI^{\lambda}D^{\mu}$ surface sliding mode controller. The fractional-order differentiator can be defined by a general fundamental operator ${}_aD^{\alpha}_t$ as a generalization of the differential and integral operators, which is defined in ref. [46]. Then, a $PI^{\lambda}D^{\mu}$ sliding surface is designed as follows:

$$\sigma = S_p\left(\theta_t - \theta_r\right) + S_iD^{-\lambda}\left(\theta_t - \theta_r\right) + S_dD^{\mu}\left(\theta_t - \theta_r\right) \tag{27}$$

where S_p, S_i, S_d, λ, and μ are adjustable control parameters, which are chosen by the designer. Equation (27) can be rewritten as follows:

$$\sigma = S_p\left(\theta_t - \theta_r\right) + S_iD^{-\lambda}\left(\theta_t - \theta_r\right) + S_dD^{\mu-1}\left(\dot{\theta}_t - \dot{\theta}_r\right) \tag{28}$$

Differentiating both sides of Eq. (28) and replacing (26) in (28) yield

$$\begin{aligned} \dot{\sigma} &= S_p\left(x_2 - \dot{\theta}_r\right) + S_iD^{1-\lambda}\left(\theta_t - \theta_r\right) + S_dD^{\mu-1}\left(a\,\cos\left(x_1\right) + cx_2 + b\left(u + V_d\right) + z + \Gamma^d_{F_m} - \ddot{\theta}_r\right) \\ &= S_p\left(x_2 - \dot{\theta}_r\right) + S_iD^{1-\lambda}\left(\theta_t - \theta_r\right) + S_dD^{\mu-1}\left(a\,\cos\left(x_1\right) + cx_2 + bu + \frac{\delta\left(x,t\right)}{S_d} + z + \Gamma^d_{F_m} - \ddot{\theta}_r\right) \end{aligned} \tag{29}$$

where $\delta\left(x,t\right)$ represents the disturbance term that is defined as follows:

$$\delta\left(x,t\right) = S_dbV_{\mathrm{d}} + \Gamma^d_{F_m} \tag{30}$$

The control input is split into three parts, namely u_{eq}, u_n, and u_s

$$u = u_{eq} + u_n + u_{\mathrm{s}} \tag{31}$$

https://doi.org/10.1017/S0263574718000802 Published online by Cambridge University Press

where u_{eq} and u_n are used to compensate the known terms and disturbance δ, respectively, while the discontinuous component of the control law u_s with its smooth approximation is used to reduce the chattering phenomenon at the sliding phase in the SMC. The uncertainty is estimated by the disturbance observer and the opposite value of the disturbance (δ) in u_n is, then, used to eliminate the effect of uncertainty. Indeed, the estimation of the uncertainty is an important part of the proposed control scheme. In the following, it is considered that the estimation of δ is available and it is donated by $\hat{\delta}$. Uncertainty estimation method will be explained in Section 3.2.5, in which a disturbance observer is used to estimate δ. The equivalent control law can be obtained by setting $\dot{\sigma}$ equal to zero:

$$u_{eq} = -\frac{1}{b}\Bigg(D^{1-\mu}\left(\frac{S_p}{S_d}\left(x_2 - \dot{\theta}_r\right)\right) + D^{2-\lambda-\mu}$$
$$\left(\frac{S_i}{S_d}(\theta_t - \theta_r)\right) + a\,\cos(x_1) + cx_2 + z - \ddot{\theta}_r + \frac{k_s}{S_d}\sigma\Bigg) \tag{32}$$

The disturbance rejection and switching control law can be defined as follows:

$$u_n = -\frac{1}{bS_d}\hat{\delta} \tag{33}$$

$$u_s = -\frac{1}{bS_d}k_{st}\ \mathrm{sat}\,(\sigma) \tag{34}$$

$$\mathrm{sat}\,(\sigma) = \begin{cases} sgn\ \sigma & if \quad |\sigma| \geq \varphi \\ \frac{\sigma}{\varphi} & if \quad |\sigma| < \varphi \end{cases} \tag{35}$$

where in (35) k_s and k_{st} are adjustable positive constants. The equivalent control laws for PID, PD, and PD surfaces are derived in the Appendix. Substituting (31), and (32) into (29), results in

$$\dot{\sigma} = -k_s\sigma + \delta + bS_d u_n + bS_d u_s \tag{36}$$

Replacing (33) and (34) in (36), the dynamics of the sliding surface is obtained as follows:

$$\dot{\sigma} = -k_s\sigma - k_{st}\ \mathrm{sat}\,(\sigma) + \delta \tag{37}$$

In (37), $\tilde{\delta} = \delta - \hat{\delta}$ is the disturbance estimation error. If the disturbance estimation ($\hat{\delta}$) is such that the estimation error ($\tilde{\delta}$) goes close to zero, the sliding surface σ will go close to zero; thereby, the sliding mode condition is satisfied. Therefore, in spite of the link deflection, the reference trajectory, which is generated by the target impedance block, will be tracked. In the next subsections, a disturbance observer is proposed to estimate the disturbance (δ).

3.2.5. Disturbance observer. In this section, a disturbance observer is designed to estimate δ such that the estimation error $\tilde{\delta}$ tends to zero. This disturbance observer is a modified version of that presented in ref. [47]. Let the estimate of the uncertainty δ be expressed by the following equation:

$$\hat{\delta} = \hat{d}\,(t) + p\,(\sigma) \tag{38}$$

where $\hat{d}\,(t)$ and $\hat{\delta}$ are an updated law that can be considered as the internal state of the observer and the estimate of the disturbance, respectively, and $p\,(\sigma)$ may be a linear or nonlinear scalar function of σ. The $\hat{d}\,(t)$ should be selected in such a way that the $\hat{\delta}$ approaches δ, and thereby, the estimation error goes to zero. Differentiating both sides of Eq. (38) and substituting $\dot{\sigma}$ from (36) yield

$$\dot{\hat{\delta}} = \dot{\hat{d}}\,(t) + \frac{\partial p}{\partial \sigma}\,(-k_s\sigma + \delta + bS_d u_n + bS_d u_s) \tag{39}$$

https://doi.org/10.1017/S0263574718000802 Published online by Cambridge University Press

The dynamics of $\hat{d}(t)$ is considered as follows:

$$\dot{\hat{d}}(t) = -\frac{\partial p}{\partial \sigma}\left(-k_s\sigma + \hat{\delta} + bS_d u_n + bS_d u_s\right) \tag{40}$$

Therefore, the dynamics of $\hat{\delta}$ can be obtained as follows:

$$\dot{\hat{\delta}} = \frac{\partial p}{\partial \sigma}\tilde{\delta} \tag{41}$$

Subtracting both sides of (41) from $\dot{\delta}$ yields

$$\dot{\tilde{\delta}} = -\frac{\partial p}{\partial \sigma}\tilde{\delta} + \dot{\delta} \tag{42}$$

For the stability of $\tilde{\delta}$, the $p(\sigma)$ must be chosen such that $\frac{\partial p}{\partial \sigma}$ be a positive function and the derivative of δ to be bounded as follows:

$$\left|\dot{\delta}\right| < \gamma \tag{43}$$

where γ represents a positive number. In the following section, the stability analysis of closed-loop system and the boundedness of $\tilde{\delta}$ and σ will be explained.

4. Stability Analysis of Closed-Loop Control System

In this section, the stability condition of closed-loop control system was taken from ref. [48]. For stability analysis a candidate Lyapunov function is considered as follows:

$$V\left(\sigma, \tilde{\delta}\right) = \frac{1}{2}\left(\sigma^2 + \tilde{\delta}^2\right) \tag{44}$$

Taking the time derivative from both sides of (44) and using (37) and (42) yield

$$\dot{V}\left(\sigma, \tilde{\delta}\right) = -k_s\sigma^2 - k_{st}\ sat\left(\sigma\right)\sigma + \tilde{\delta}\dot{\delta} + \tilde{\delta}\sigma - \frac{\partial p}{\partial \sigma}\tilde{\delta}^2 \tag{45}$$

Using Young's inequality, $\tilde{\delta}\sigma \leq \frac{1}{2}\left(\tilde{\delta}^2 + \sigma^2\right)$, $\tilde{\delta}\dot{\delta} \leq \frac{1}{2}\left(\tilde{\delta}^2 + \dot{\delta}^2\right)$ and (43), Eq. (45) can be rewritten as follows:

$$\dot{V}\left(\sigma, \tilde{e}\right) \leq -\left(k_s - \frac{1}{2}\right)\sigma^2 - \left(\frac{\partial p}{\partial \sigma} - 1\right)\tilde{\delta}^2 + \frac{1}{2}\gamma^2 - k_{st}\ sat\left(\sigma\right)\sigma \tag{46}$$

The control parameter can be chosen such that $\left(k_s - \frac{1}{2}\right)$ and $\left(\frac{\partial p}{\partial \sigma} - 1\right)$ are always positive. From (46), it can be proven that the dynamics of σ and the uncertainty estimation error $\tilde{\delta}$ are not asymptotically stable but ultimately bounded.[49] The upper bounds of $\left|\tilde{\delta}\right|$ and $|\sigma|$ can be obtained from (47) and (48), respectively

$$\left|\tilde{\delta}\right| \leq \beta = \frac{\gamma}{\sqrt{2\left(\frac{\partial p}{\partial \sigma} - 1\right)}} \tag{47}$$

https://doi.org/10.1017/S0263574718000802 Published online by Cambridge University Press

$$|\sigma| \leq \frac{\beta + \sqrt{\beta^2 + 4k_s\gamma}\beta}{2k_s} \tag{48}$$

Therefore, from (47) and (48), the uncertainty estimation error $\tilde{\delta}$ and σ are ultimately bounded, and the control parameter such as $\frac{\partial p}{\partial \sigma}$, k_s, and k_{st} can be chosen so that the bounds on $\left|\tilde{\delta}\right|$ and $|\sigma|$ can be made sufficiently small.

5. Performance Criteria

In this section, the following performance criteria are defined in order to evaluate the performance of the controller:

- Root mean squared error (RMSE) for the trajectory tracking in the constrained and free motion phases:

$$\text{RMSE} = e_p + e_f \tag{49}$$

where

$$e_p = \sqrt{\sum_{t=0}^{t_c} \|\theta_d(t) - \theta_t(t)\|^2 T/t_f}.$$

and

$$e_f = \sqrt{\sum_{t=tp}^{t_f} \|F_d(t) - F_e(t)\|^2 T/t_f}.$$

represent the error value in the free motion and in the constrained motion mode, respectively.

- Root mean square value (RMSV) of the control input voltage:

$$\text{RMSV} = \sqrt{\sum_{0}^{t_f} \|u(t)\|^2 T/t_f} \tag{50}$$

Both RMSE and RMSV are used as objective numerical measures of tracking performance for an entire error curve, where T is the sample time, t_c is the collision time, and t_f and $t_p \in \left(t_c, t_f\right)$ represent the total running time of the simulations and a definite time in the collision phase, respectively. In our simulation, these parameters are chosen as, $T = 1 \times 10^{-3}$ s, $t_c = 3$ s, $t_f = 10$ s, and $t_p = 4.5$ s. The criterion RMSV shows the consumption of energy.

6. Simulation Results

6.1. Simulation results for the constrained and unconstrained motion phases

Numerical simulations have performed using the SIMULINK. To solve the sets of fractional-order differential equations related to the sliding mode controller in the inner loop position control and the dynamics of the system, the CRONE Toolbox and Runge–Kutta solver with a fixed step size of 0.001 are used. Table I shows physical parameters of the system (block I), which most of them were taken from refs. [19] and [44]. Table II depicts the control parameters of impedance control and inner loop position control (block III). The control parameters have been chosen by trial and error so that the closed-loop control system would be stable. However, this parameter may be optimized by optimization approaches such as genetic algorithms (GAs).

In the following, the simulation has been carried out for constrained and unconstrained motions, in the presence of the Coulomb friction disturbances. In the constrained phase, the desired contact force

https://doi.org/10.1017/S0263574718000802 Published online by Cambridge University Press

Table I. Physical parameters of the system[19].

Parameter	Description	Value
Data of the flexible arm		
E	Young's modulus	271×10^9 Pa
I	Cross-sectional inertia	3.017×10^{-12} m^4
ρ	Density	1800 kg/m^3
l	Length	0.98 m
d	Diameter	2.8×10^{-3} mm
m	Tip mass	43.71×10^{-3} kg
ξ	Friction coefficient	0.00765
K_1	Rotational stiffness coefficient	0.385
K_3	Rotational stiffness coefficient	0.0225
g	Gravitational acceleration	9.8 m/s^2
Data of the motor-gear set		
J	Total motor inertia + reduction gear	6.87×10^{-5} kg m^2
v	Viscous friction	1.041×10^{-3} kg m^2/s
n	Reduction ratio of the motor gear	50
K	Motor constant	2.1×10^{-1} N m/V
V_{sat}	Saturation voltage of the servo amplifier	± 10 V
Data of the environment		
k_e	Stiffness	100 N/m
v_e	Damping coefficient	1 N s/m

Table II. Control parameters of the system.

Parameter	Description	Value
Characteristics of the target impedance		
k_p	Target value for the stiffness	k_p^*
k_d	Target value for the damping coefficient	$\frac{k_p^*}{5}$
k_m	Target value for the inertia coefficient	$\frac{k_p^*}{100}$
Characteristics of FSMC		
S_p	Non-negative coefficient for the proportional term	5
S_i	Non-negative coefficient for the integral term	1
S_d	Non-negative coefficient for the derivative term	1
μ	Fractional order for the PD^μ and the $PI^\lambda D^\mu$	0.9
λ	Fractional order for the $PI^\lambda D^\mu$	0.9
k_s	Positive constant for the feedback control gain	1
k_{st}	Switching feedback control gain	0.5
$\frac{\partial p}{\partial \sigma}_1$	Control parameter for the unconstrained phase	10
$\frac{\partial p}{\partial \sigma}_2$	Control parameter for the constrained phase	10
Characteristics of hypothetical object		
k_e^*	Stiffness of the hypothetical environment	10 N/m
v_e^*	Damping coefficient of the hypothetical environment	1 Ns/m

has been chosen equal to 20 N ($F_d = 20$ N), and in the unconstrained phase, the desired trajectory has been defined as the following equation:

$$\theta_d(t) = \begin{cases} 5t^2; & 0 \le t < 1 \\ 10t - 5\ ; & 1 \le t < 3 \\ 10\left(4t - \frac{t^2}{2}\right) - 50; & 3 \le t < 4 \\ 30; & t \ge 4 \end{cases} \tag{51}$$

The simulation results are provided for the PD SMC, the PID SMC, the PD^μ SMC, and the $PI^\lambda D^\mu$ SMC controllers used in the inner loop position control scheme.

https://doi.org/10.1017/S0263574718000802 Published online by Cambridge University Press

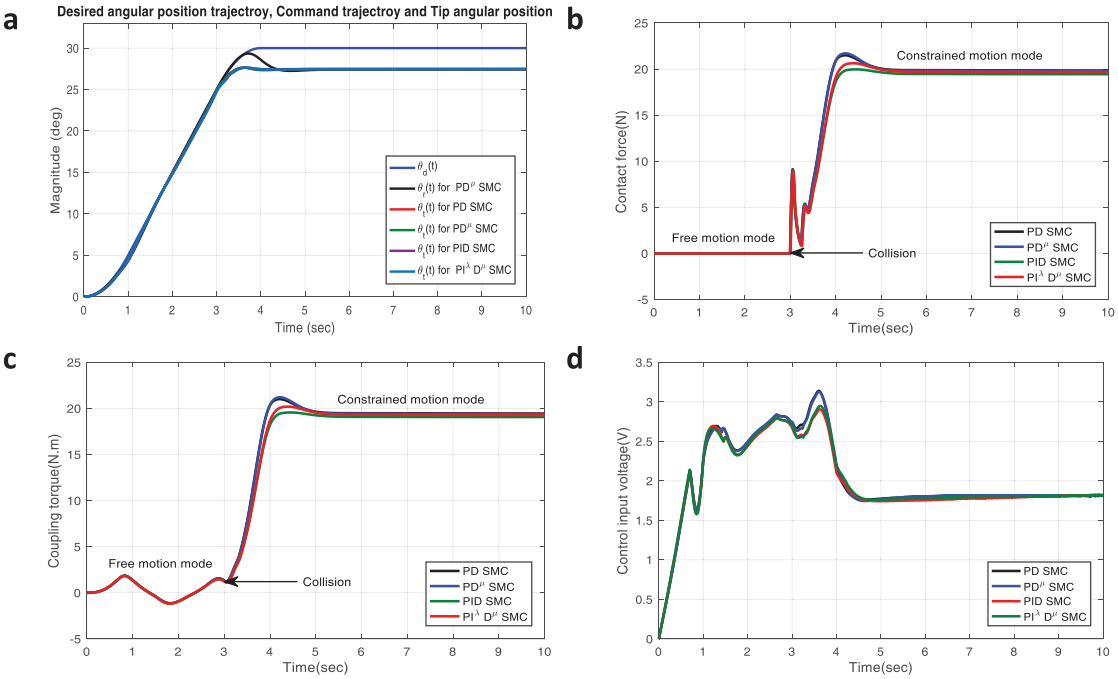

Fig. 7. Transient response of the system for both constrained and unconstrained motions phase. (a) simulation of the desired trajectory tracking (position control), (b) simulation of the desired contact force regulating (force control), (c) simulation of the coupling torque, and (d) simulation of the control input voltage.

6.1.1. Simulation results for the PD, the PD$^{\mu}$, the PID, and the PI$^{\lambda}$D$^{\mu}$ surface sliding mode controllers. Figure 7 illustrates the transient response of the system for both constrained and unconstrained motions phase. Figure 7(a) shows the desired trajectory tracking (position control in the free motion phase). Figure 7(b) depicts the transient response of the desired contact force regulating (force control in the constrained motion phase). Figure 7(c) shows the coupling torque applied to the beam. Figure 7(d) illustrates the control input voltage to the DC motor.

As can be seen in Fig. 7(a) and (b), before the contact ($t < 3$ s), the tip angle follows the desired trajectory and the contact force is zero. In this case, the system is controlled in free motion phase and the impedance controller acts as a position controller until the collision with the environment is detected at time $t = 3$ s. After the impact detection, the system is controlled in constrained phase (during the contact ($t > 3$ s)). In this situation, the impedance controller acts as a regulating force controller and the controller immediately stabilizes the system to track the reference trajectory (desired contact force) with null steady-state error. As shown in Fig. 7(d), the control effort is very small and never saturates the amplifier that supplies the motor at 10 and -10 V, providing a smooth trajectory tracking without overheating the electrical system. In order to compare the performance of the proposed controllers, the results of simulation are summarized in Table III. It can be seen that the proposed fractional-order surface SMC (PD^{μ} and $PI^{\lambda}D^{\mu}$) has the smaller error, better tracking and robustness capabilities than the classical sliding mode controllers (PD SMC and PID SMC) specially in constrained motion phase. However, the computational complexity of the proposed fractional controller is more than its integer order counterpart, which is computationally simple.

According to Table III, the fractional-order sliding mode controllers relatively outperformed the conventional sliding mode controllers. Therefore, in the following subsections, we prefer to perform the rest of simulations by using the proposed fractional-order surface PD^{μ} SMC.

6.2. Simulation results for the constrained motion with different values of the environment parameters

In this section, first, the simulations were performed for different values of the environment stiffness (we assume $v_e = 1\ \frac{Ns}{m}$). Then, the simulations were performed for different values of the environment

https://doi.org/10.1017/S0263574718000802 Published online by Cambridge University Press

Table III. Simulation results of the proposed controllers performances, in presence of the Coulomb friction disturbances.

Inner loop position control strategy	e_p	e_f	RMSE	RMSV
PDSMC	0.2641	0.2388	0.5029	2.0839
PD$^{\mu}$SMC	0.2673	0.1968	0.4640	2.0799
PIDSMC	0.2849	0.5166	0.8014	2.0436
PI$^{\lambda}$D$^{\mu}$SMC	0.2849	0.3056	0.5905	2.0568

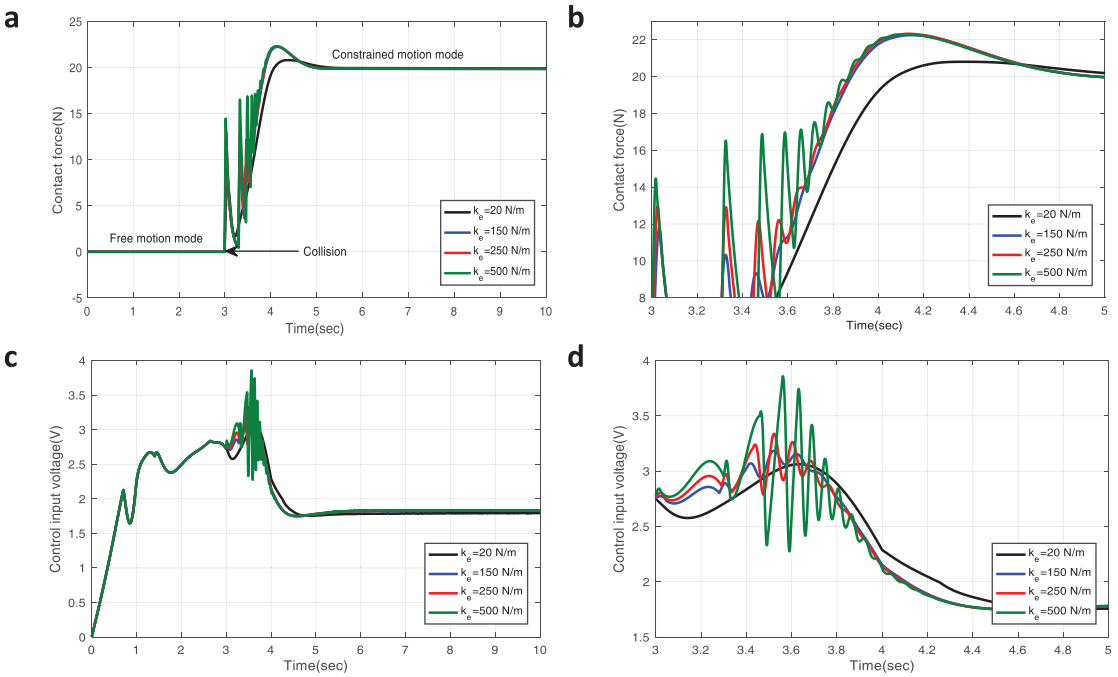

Fig. 8. Transient response of the system for constrained motion phase with different values of the environment stiffness. (a) Simulation of the desired contact force regulating, (b) detail of subfigure (a), (c) simulation of the control input voltage, and (d) detail of subfigure (c).

damping coefficient (we assume $k_e = 100\ \frac{N}{m}$) in order to illustrate the robustness of the proposed control strategy against changes in the environment parameters. Figures 8 and 9 show the simulation results for different values of stiffness and damping coefficient, respectively.

As it can be observed from Figs. 8 and 9, there is a slight oscillation in the collision phase with smaller values of the stiffness and damping coefficient of the environment (very soft environment). However, these oscillations will disappear by increasing the stiffness and damping coefficient of the environment. Moreover, the system response is stable against variations in the stiffness of the environment.

6.3. Simulation results for different values of the stiffness of hypothetical environment

In this section, in order to show robustness of the controller several simulations are performed for different values of the stiffness of hypothetical environment (k_e^*).

As shown in Fig. 10, the transient response of the system for both constrained and unconstrained motions mode is valid for the different values of the stiffness of the hypothetical environment and the controller makes sure to be robust against the uncertainty of the environment.

6.4. Simulation results for the constrained motion with possible variations in payload and viscous friction

In this section, effects of changes in the payload (m) and viscous friction (v) in the system response have been investigated. This payload variations can be occurred, for instance, due to the use of various

https://doi.org/10.1017/S0263574718000802 Published online by Cambridge University Press

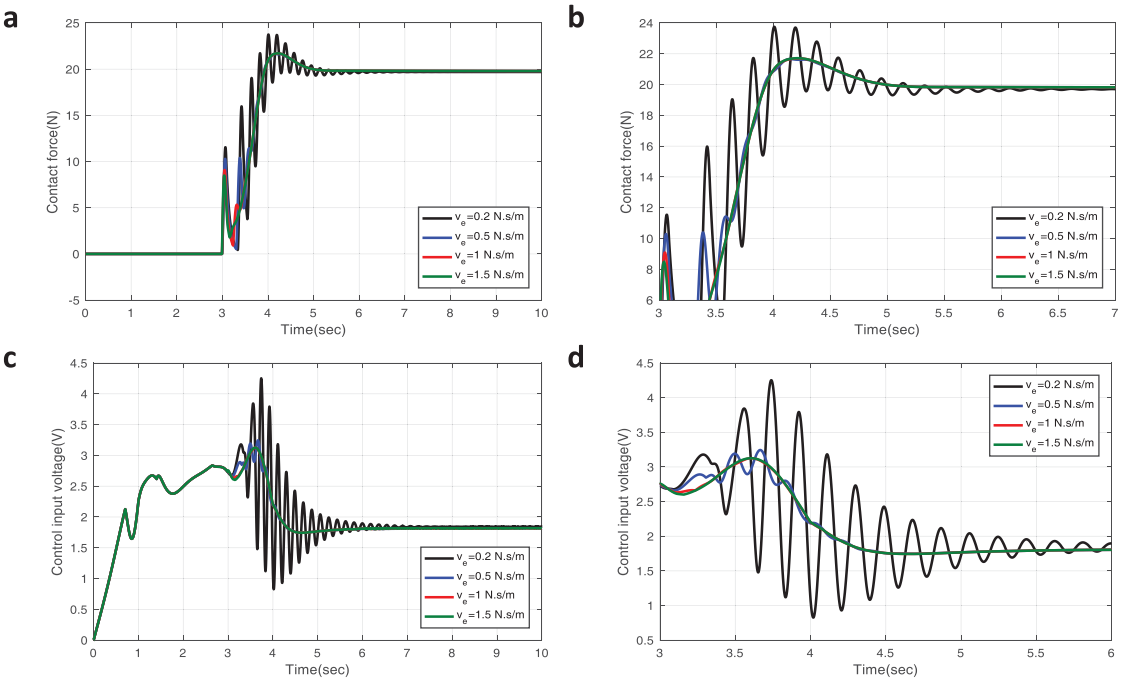

Fig. 9. Transient response of the system for constrained motion phase with different values of the environment damping coefficient. (a) Simulation of the desired contact force regulating, (b) detail of subfigure (a), (c) simulation of the control input voltage, and (d) detail of subfigure (c).

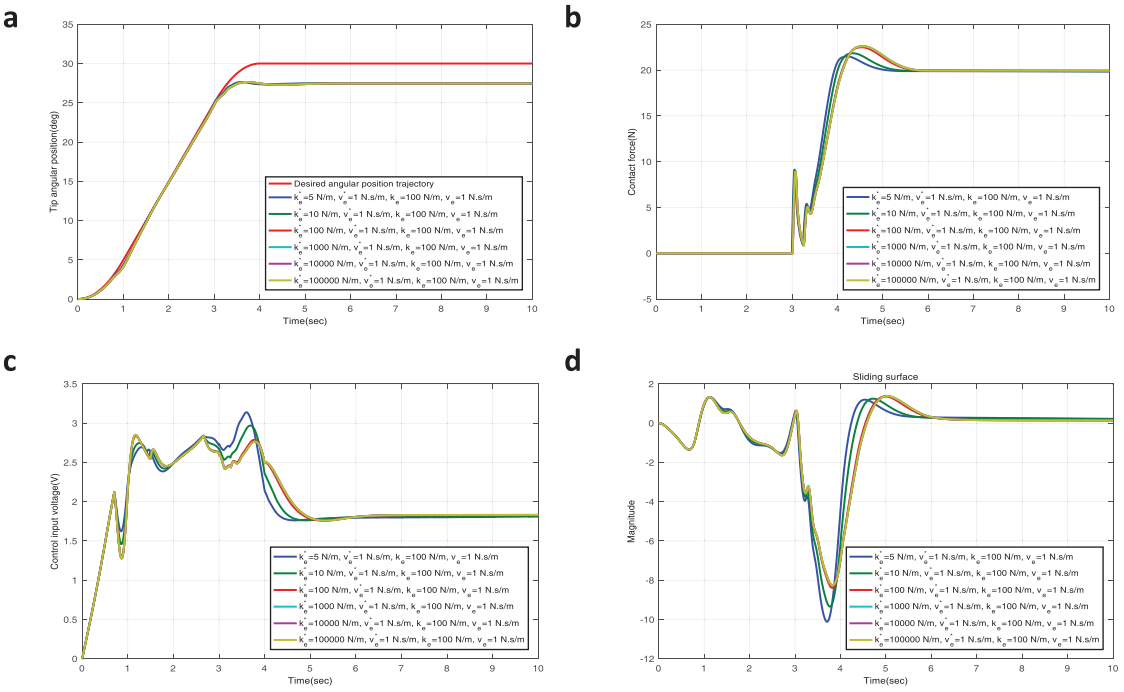

Fig. 10. Transient response of the system for both constrained and unconstrained motions phases. (a) Simulation of the desired trajectory tracking (position control), (b) simulation of the desired contact force regulating (force control), (c) simulation of the control input voltage, and (d) simulation of the sliding surface.

tools placed at the end-effector of the manipulator. A range of possible payload values ($m_n \pm 0.25m_n$, $m_n = 0.044$ kg being the nominal value) have been chosen so that the arm could support under normal operating condition. Robustness of the control system has also been studied under variations

https://doi.org/10.1017/S0263574718000802 Published online by Cambridge University Press

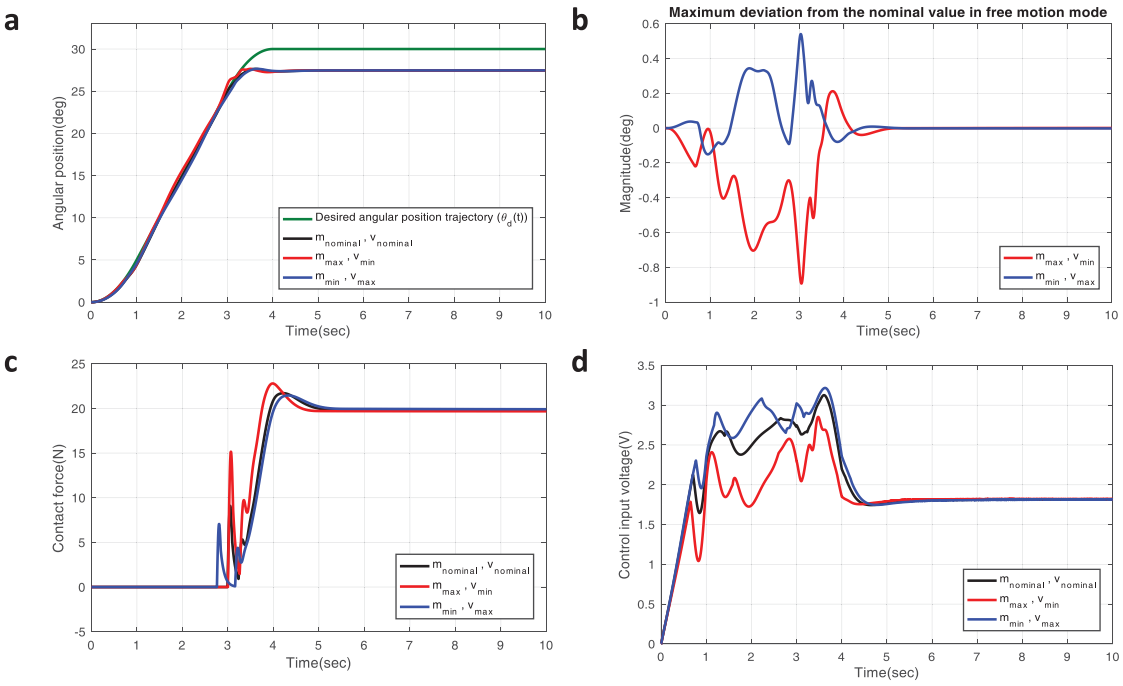

Fig. 11. Transient response of the system for constrained motion phase when payload and viscous friction vary simultaneously in the defined range. (a) Simulation of the desired trajectory tracking (position control), (b) maximum deviation from the nominal value in free motion mode, (c) simulation of the desired contact force regulating, and (d) simulation of the control input voltage.

in the viscous friction parameter ($v_n \pm 0.25v_n$, $v_n = 1.041 \times 10^{-3}$ kg m$^2/s$ being the nominal value). The other remaining parameters of the system have been assumed unchanged. Figure 11 shows the simulation results when both parameters vary at the same time in the defined range.

As can be seen from Fig. 11(a) and (b), the maximum deviation of the system response with respect to the nominal case (m_n, v_n) in free motion phase is 0.9 ° when m is equal to $m_{\max} = m_n + 0.25m_n$ and v is equal to $v_{min} = v_n - 0.25v_n$. From Fig. 11(c), it is obvious that the steady state error is near to zero and there is no deviation of the system response with respect to the nominal case in constrained motion phase. As can be illustrated in Fig. 11(d), the control input voltage is smooth and never exceed the saturation voltage of the amplifier in both free and constrained motions mode.

6.5. Simulation results for the FSMC equipped with disturbances observer and the conventional SMC

In this section, in order to investigate the capability of the FSMC equipped with disturbance observer (the proposed control approach) in comparison with the conventional SMC without disturbances observer, several simulations are carried out for both constrained and unconstrained motion modes.

Figure 12 illustrates the transient response of the system for both constrained and unconstrained motions phase. Figure 12(a) shows the desired trajectory tracking (position control in the free motion phase). Figure 12(b) depicts the transient response of the desired contact force (force control in the constrained motion phase). Figure 12(c) and (d) shows the control input voltage to the DC motor and the sliding surface, respectively.

As can be illustrated from Fig. 12, the FSMC equipped with disturbance observer used in inner loop position control block (black curve) outperformed the conventional SMC without disturbance observer in both free and constrained motions modes. In the free motion mode, as shown in Fig. 12(a), the tip angular position (black curve) follows completely the desired angular position trajectory. Whereas, the simulation result of the conventional SMC shows that the tip angular position (red curve) is unable to track the desired angular position trajectory. In the constrained motion phase, as shown in Fig. 12(b), the contact force is regulating to its desired value without any steady state error. However, the conventional SMC simulation result shows that the contact force oscillates around the desired value

https://doi.org/10.1017/S0263574718000802 Published online by Cambridge University Press

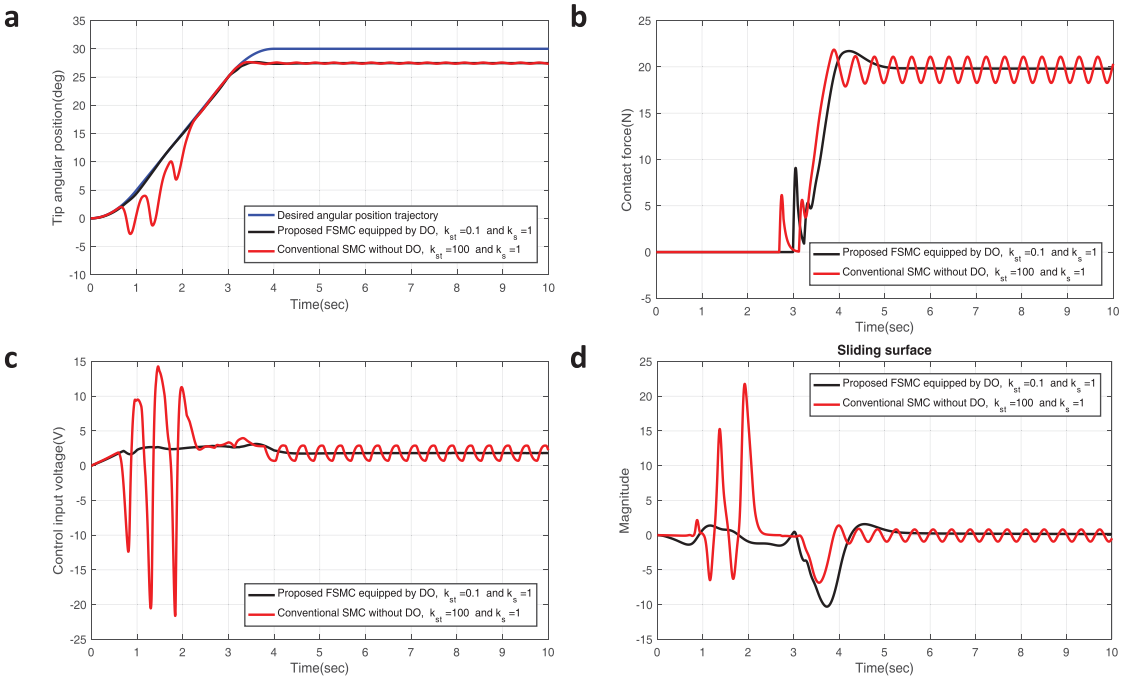

Fig. 12. Transient response of the system for both constrained and unconstrained motions phase. (a) Simulation of the desired trajectory tracking (position control), (b) simulation of the desired contact force regulating (force control), (c) simulation of the control input voltage, and (d) simulation of the sliding surface.

in the steady state. As shown in Fig. 12(c), the control input voltage obtained in the proposed control method is much smoother and with less oscillations amplitude than the control input voltage is obtained from the conventional SMC. It should be noted that, the disturbance observer used in the FSMC, compensates the input disturbance caused by the flexibility of the link in addition to compensation parameter uncertainties and Coulomb friction disturbances. Thus, the proposed FSMC equipped with disturbance observer has better performance as compared with the conventional SMC in both free and constrained motions mode. Moreover, as shown in Fig. 12(d), the chattering phenomenon has been eliminated by using the proposed control approach along with the use of the smoothing function ($sat(\sigma)$) in the control law.

7. Conclusion

A robust impedance control for a single-link flexible manipulator has been designed by using the FSMC scheme under unknown environment. The FSMC is also equipped with a disturbance observer. First, the nonlinear dynamics model of the tip angle is derived based on a lumped masses model in the constrained motion phase. A unified control strategy is, then, designed based on this nonlinear model. The main contribution of this work is that only one model is used to design the controller, which is valid for both constrained and unconstrained motions. Thus, without needing a separate algorithm to detect collision between link and the environment, the controller switches automatically from the free motion to the constrained motion phase. In this regard, the position-based impedance control system is proposed with force tracking. The precise design of the inner loop position controller is the important part of impedance control. Therefore, primarily a classical sliding mode controller is designed for the inner loop position control. The work is, then, followed by using a fractional-order sliding mode controller. The combination of the fractional control and the SMC equipped with a disturbance observer is used to improve the performance of the system response. This hybrid system makes the system more robust against uncertainties and disturbances. The simulation results demonstrate the significance of the proposed control approach in both free motion and constrained motions modes where the flexible link interacting with unknown environment. Moreover, the proposed control scheme is robust against the parameter variations of environment, payload and viscous friction

https://doi.org/10.1017/S0263574718000802 Published online by Cambridge University Press

variations, and input disturbances. Such that with 25% variation in parameters of the system, in the free motion mode, the maximum deviation from the nominal value is 0.9 °. In the constrained motion mode, the steady-state error of the desired contact force regulating is zero. Besides, the control input voltage is smooth and never saturates the amplifier that supplies the motor at 10 and −10 V. Therefore, this feature makes the practical implementation of the proposed control approach to be feasible.

Conflicts of Interest

The authors declared no potential conflicts of interest with respect to the research, authorship, and/or publication of this paper.

Funding

The author(s) received no financial support for the research, authorship, and/or publication of this paper.

References

1. S. K. Dwivedyć and P. Eberhard, "Dynamic analysis of flexible manipulators, a literature review," *Mech. Mach. Theory* **41**(7), 749–777 (2006).
2. F. Wangć and Y. Gao, *Advanced Studies of Flexible Robotic Manipulators, Modeling, Design, Control and Applications* (World Scientific, New Jersey, 2003) ISBN: 978-981-279-672-1.
3. O. Sawodny, H. Aschemann and A. Bulach, "Mechatronical Designed Control of Fire Rescue Turnable Ladders as Flexible Link Robots," *Proceedings of the IFAC 15th Triennial World Congress* (2002).
4. D. Feliu-Talegon and V. Feliu-Batlle, "Improving the position control of a two degrees of freedom robotic sensing antenna using fractional-order controllers," *Int. J. Control* **90**, 1256–1281 (2017).
5. V. Feliu-Batlle, D. Feliu-Talegon and C. F. Castillo-Berrio, "Improved object detection using a robotic sensing antenna with vibration damping control," *Sensors* **17**(4), 1–28 (2017).
6. R. A. Beasley and R. D. Howe, "Model-Based Error Correction for Flexible Robotic Surgical Instruments," **In**: *Proceedings of the Robotics, Science and Systems I* (Massachusetts Institute of Technology, Cambridge, MA, 2005).
7. N. Hogan, "Impedance control: An approach to manipulation: Part1, Part2, Part3," *J. Dyn. Syst. Meas. Control* **107**, 1–24 (1985).
8. M. M. Fateh and R. Babaghasabha, "Impedance control of robots using voltage control strategy," *Nonlinear Dyn.* **74**(1), 277–286 (2013).
9. D. Heck, A. Saccon, N. V. D. Wouw and H. Nijmeijer, "Guaranteeing stable tracking of hybrid position-force trajectories for a robot manipulator interacting with a stiff environment," *Automatica* **63**, 235–247 (2016).
10. S. Jung, T. C. Hsia and R. G. Bonitz, "Force tracking impedance control of robot manipulators under unknown environment," *IEEE Trans. Control Syst. Technol.* **12**(3), 474–483 (2004).
11. T. Lasky and T. C. Hsia, "On Force-Tracking Impedance Control of Robot Manipulators," *Proceedings of the IEEE International Conference on Robotics and Automation* (1991) pp. 274–280.
12. S. Lee and H. S. Lee, "Intelligent Control of Manipulators Interfacing with an Uncertain Environment Based on Generalized Impedance," *Proceedings of the IEEE Symposium on Intelligent Control* (1991) pp. 61–66.
13. H. Seraji and R. Colbaugh, "Force Tracking in Impedance Control," *Proceedings of the IEEE International Conference on Robotics and Automation* (1993) pp. 499–506.
14. M. Sharifi, S. Behzadipour and G. R. Vossoughi, "Nonlinear model reference adaptive impedance control for human-robot interactions," *Control Eng. Pract.* **32**, 9–27 (2014).
15. Q. Xu, "Robust impedance control of a compliant microgripper for high-speed position/force regulation," *IEEE Trans. Ind. Electron.* **62**(2), 1201–1209 (2015).
16. C. F. Castillo-Berrio and V. Feliu-Batlle, "Vibration-free position control for a two degrees of freedom flexible-beam sensor," *IEEE Trans. Ind. Electron.* **27**, 1–12 (2015).
17. C. F. Castillo-Berrio, S. N. Engin and V. Feliu-Batlle, "A study on the tip tracking control of a single flexible beam," *Trans. Inst. Meas. Control* **38**(5), 602–617 (2017).
18. G. Mamani, J. Besedas and V. Feliu, "Sliding mode tracking control of a very lightweight single-link flexible robot robust to payload changes and motor Friction," *J. Vib. Control* **18**(8), 1141–1155 (2012).
19. I. Payo, V. Feliu and O. D. Cortazar, "Force control of a very lightweight single-link flexible arm based on coupling torque feedback," *Mechatronics* **19**(3), 334–347 (2009).
20. G. R. Vossoughi and A. Karimzadeh, "Impedance control of a flexible link robot for constrained and unconstrained maneuvers using sliding mode control (SMC) method," *Sci. Iran.* **14**(1), 33–45 (2007).
21. T. Wongratanaphisan and M. O. T. Cole, "Robust impedance control of a flexible structure mounted manipulator performing contact tasks," *IEEE Trans. Robot.* **25**(2), 445–451 (2009).

22. Z. H. Jiang, "Impedance control of flexible robot arms with parametric uncertainties," *J. Intell. Robot. Syst.* **42**(2), 113–133 (2005).
23. A. Benosman and G. L. Vey, "Control of flexible manipulators: A survey," *Robotica* **22**(5), 533–545 (2004).
24. L. Marinangeli, F. Alijani and S. H. HosseinNia, "A fractional-order positive position feedback compensator for active vibration control," *IFAC-PapersOnLine* **50**(1), 12809–12816 (2017).
25. L. Marinangeli, F. Alijani and S. H. HosseinNia, "Fractional-order positive position feedback compensator for active vibration control of a smart composite plate," *J. Sound Vib.* **412**, 1–16 (2018).
26. S. H. HosseinNia, Inés. Tejado, D. Torres and B. M. Vinagre, "Vibration Suppression Controller for a Flexible Beam on a Cart using SMC," *Proceedings of the 1st Iberian Robotics Conference* (2014) pp. 127–139.
27. Y. Chen, D. Xue and H. Dou, "Fractional Calculus and Biomimetic Control," *Proceedings of the IEEE International Conference on Robotics and Biomimetics* (2004) pp. 901–906.
28. Y. Chun, C. YangQuan and Z. Shou-ming, "Fractional-order sliding mode based extremum seeking control of a class of nonlinear systems," *Automatica* **50**(12), 3173–3181 (2014).
29. D. Zhang, L. Cao and S. Tang, "Fractional-order sliding mode control for a class of uncertain nonlinear systems based on LQR," *Int. J. Adv. Robot. Syst.* **14**(2), 1–15 (2017).
30. M. O. Efe, "Fractional fuzzy adaptive sliding-mode control of a 2-DOF direct-drive robot arm," *IEEE Trans. Syst., Man, Cybern., Part B (Cybern.)* **38**(6), 1561–1570 (2008).
31. A. Fayazi and H. Nabizadeh-Rafsanjani, "Fractional Order Fuzzy Sliding Mode Controller for Robotic Flexible Joint Manipulators," *Proceedings of the IEEE International Conference on Control and Automation* (2011) pp. 1244–1249.
32. N. M. Fonseca Ferreira and J. A. Tenreiro Machado, "Fractional-Order Hybrid Control of Robotic Manipulators," *Proceedings of the 11th International Conference on Advanced Robotics* (2003) pp. 393–398.
33. I. Ghasemi, A. Ranjbar-Noei and J. Sadati, "Sliding mode based fractional-order iterative learning control for a nonlinear robot manipulator with bounded disturbance," *Trans. Inst. Meas. Control* **38**, 1–12 (2016).
34. L. Heng, P. Yongping, L. Shenggang and Y. E. Chen, "Synchronization for fractional-order neural networks with full/under-actuation using fractional-order sliding mode control," *Int. J. Mach. Learn. Cybern.* **8**, 1–14 (2017).
35. S. H. HosseinNia, R. Ghaderi, M. Mahmoudian and S. Momani, "Sliding mode synchronization of an uncertain fractional order chaotic system," *Comput. Math. Appl.* **59**(5), 1637–1643 (2010).
36. S. H. HosseinNia, Inés. Tejado and B. M. Vinagre, "Fractional-order reset control: Application to a servomotor," *Mechatronics* **23**(7), 781–788 (2013).
37. S. H. HosseinNia, Inés. Tejado, V. Milanés, J. Villagr and B. M. Vinagre, "Experimental application of hybrid fractional-order adaptive cruise control at low speed," *IEEE Trans. Control Syst. Technol.* **22**(6), 2329–2336 (2014).
38. M. E. Krijnen, R. A. van-Ostayen and S. H. HosseinNia, "The application of fractional order control for an air-based contactless actuation system," *ISA Trans.* (2017) doi: 10.1016/j.isatra.2017.04.014.
39. C. Ma and Y. Hori, "Fractional-order control: Theory and applications in motion control," *IEEE Ind. Electron. Mag.* **1**(4), 6–16 (2007).
40. I. Tejado, S. H. HosseinNia and B. M. Vinagre, "Adaptive gain-order fractional control for network-based applications," *Fractional Calculus Appl. Anal.* **17**(2), 462–482 (2014).
41. E. Bayo, "A finite-element approach to control the end-point motion of a single-link flexible robot," *J. Robot. Syst.* **4**(1), 63–75 (1987).
42. V. Feliu, K. Rattan and N. Brown, " Modeling and control of single-link flexible arms with lumped masses," *J. Dyn. Syst. Meas. Control* **114**(1), 59–69 (1992).
43. R. H. Cannon and E. Schmitz, "Initial experiments on the end-point control of a flexible robot," *Int. J. Robot. Res.* **3**(3), 62–75 (1984).
44. I. Payo, F. Ramos, O. D. Cortazar and V. Feliu, "Experimental Validation of Nonlinear Dynamic Models for Single-Link Very Flexible Arms," *Proceedings of the IEEE Conference on Decision and Control, and the European Control Conference* (2005) pp. 5304–5309.
45. S. H. HosseinNia, Inés. Tejado, B. M. Vinagre and D. Sierociuk, "Boolean-based fractional order SMC for switching systems: Application to a DC-DC buck converter," *Signal, Image Video Process.* **6**(3), 445–451 (2012).
46. A. Calderon, B. Vinagre and V. Feliu, "Fractional order control strategies for power electronic buck converters," *Signal Process.* **86**(10), 2803–2819 (2006).
47. W. H. Chen, "Nonlinear disturbance observer-enhanced dynamic inversion control of missiles," *J. Guid., Control Dyn.* **26**(1), 161–166 (2003).
48. V. S. Deshpande, B. Mohan, P. D. Shendge and S. B. Phadke, "Disturbance observer based sliding mode control of active suspension systems," *J. Sound Vib.* **333**(11), 2281–2296 (2014).
49. M. Corless and G. Leitman, "Continuous state feedback guaranteeing uniform ultimate boundedness for uncertain dynamic systems," *IEEE Trans. Autom. Control* **26**(5), 1139–1144 (1981).

Appendix: The equivalent control law for PID, PD, and PD^{μ} surfaces

Conventional PID surface sliding mode controller

A PID sliding surface can be expressed as follows:

$$\sigma = S_p(\theta_t - \theta_r) + S_i \int (\theta_t - \theta_r)\, dt + S_d\left(\dot{\theta}_t - \dot{\theta}_r\right) \tag{A.1}$$

where S_p, S_i, and S_d are adjustable control parameters, which are chosen by designer. Differentiating both sides of Eq. (A.1) and replacing (26) in (A.1) yield

$$\begin{aligned}\dot{\sigma} &= S_i x_1 + \left(S_p + S_d c\right) x_2 + S_d a\, \cos(x_1) - \left(S_i\theta_r + S_p\dot{\theta}_r + S_d\ddot{\theta}_r\right) + bS_d\,(u + V_d) + S_d z + \Gamma_{F_m}^d \\ &= S_i x_1 + \left(S_p + S_d c\right) x_2 + S_d a\, \cos(x_1) - \left(S_i\theta_r + S_p\dot{\theta}_r + S_d\ddot{\theta}_r\right) + bS_d u + S_d z + \delta(x,t)\end{aligned} \tag{A.2}$$

Similar to the Section 3.2.4 the control input splits into three parts according to (31). u_n and u_s are obtained in accordance with Eqs. (33) and (34), respectively. The component u_{eq} is used to compensate the known terms as the following equation, which is equal to (32) when we set ($\lambda = \mu = 1$)

$$u_{eq} = -\frac{1}{b}\left(\left(\frac{S_p + S_d c}{S_d}\right) x_2 + a\, \cos(x_1) + \left(\frac{S_i}{S_d}\right) x_1 - \left(\frac{S_i}{S_d}\theta_r + \frac{S_p}{S_d}\dot{\theta}_r + \ddot{\theta}_r\right) + z + \frac{k_s}{S_d}\sigma\right) \tag{A.3}$$

Substituting (33), (34), and (A.3) in (A.2), the sliding surface dynamics is obtained as Eq. (37).

Conventional PD Surface Sliding Mode Controller

A typical PD sliding surface can be selected as follows:

$$\sigma = S_p(\theta_t - \theta_r) + S_d\left(\dot{\theta}_t - \dot{\theta}_r\right) \tag{A.4}$$

where S_p and S_d are adjustable control parameters, which are chosen by the designer. Taking the time derivative of both sides of (27) and using (26), one can obtain

$$\begin{aligned}\dot{\sigma} &= \left(S_p + S_d c\right) x_2 + S_d a\, \cos(x_1) - S_p\dot{\theta}_{\mathrm{r}} + S_d b\,(u + V_{\mathrm{d}}) - S_d\ddot{\theta}_{\mathrm{r}} + S_d \mathrm{z} + \Gamma_{F_m}^d \\ &= \left(S_p + S_d c\right) x_2 + S_d a\, \cos(x_1) - S_p\dot{\theta}_{\mathrm{r}} + S_d b u - S_d\ddot{\theta}_{\mathrm{r}} + S_d \mathrm{z} + \delta(x,t)\end{aligned} \tag{A.5}$$

As mentioned above, the control input may be split into three parts according to Eq. (31). u_n and u_s are obtained in accordance with Eqs. (32) and (33), respectively. The component u_{eq} is used to compensate the known terms as the following equation, which is equal to (32) when we select $S_i = 0$ and set $\mu = 1$.

$$u_{eq} = -\frac{1}{b}\left(\left(\frac{S_p + S_d c}{S_d}\right) x_2 + a\, \cos(x_1) - \frac{S_p}{S_d}\dot{\theta}_r - \ddot{\theta}_r + z + \frac{k_s}{S_d}\sigma\right) \tag{A.6}$$

Replacing (33), (34), and (A.6) in (A.5), the dynamics of the sliding surface is obtained, which again is equal to Eq. (37).

Fractional-Order PD^{μ} Surface Sliding Mode Controller

A PD^{μ} sliding surface can be written as follows:

$$\sigma = S_p(\theta_t - \theta_r) + S_d D^{\mu}(\theta_t - \theta_r) \tag{A.7}$$

https://doi.org/10.1017/S0263574718000802 Published online by Cambridge University Press

where S_p, S_d, and μ are adjustable control parameters, which are selected by the designer. Equation (A.7) may be rewritten as follows:

$$\sigma = S_p\left(\theta_t - \theta_r\right) + S_d D^{\mu-1}\left(\dot{\theta}_t - \dot{\theta}_r\right) \tag{A.8}$$

Taking a derivative from both sides of Eq. (A.8) and substitution of (26) in (A.8) result

$$\begin{aligned}\dot{\sigma} &= S_p\left(x_2 - \dot{\theta}_r\right) + S_d D^{\mu-1}\left(a\,\cos\left(x_1\right) + cx_2 + b\left(u + V_d\right) + z + \Gamma^d_{F_m} - \ddot{\theta}_r\right) \\ &= S_p\left(x_2 - \dot{\theta}_r\right) + S_d D^{\mu-1}\left(a\,\cos\left(x_1\right) + cx_2 + bu + \frac{\delta\left(x,t\right)}{S_d} + z + \Gamma^d_{F_m} - \ddot{\theta}_r\right)\end{aligned} \tag{A.9}$$

This reminds again, as mentioned in the two previous subsections, the control input splits into three parts according to Eq. (31). u_n and u_s are obtained in accordance with Eqs. (33) and (34), respectively. The component u_{eq} is used to compensate the known terms as the following equation, which is equal to (32) when we set $S_i = 0$

$$u_{eq} = -\frac{1}{b}\left(D^{1-\mu}\left(\frac{S_p}{S_d}\left(x_2 - \dot{\theta}_r\right)\right) + a\,\cos\left(x_1\right) + cx_2 + z - \ddot{\theta}_r + \frac{k_s}{S_d}\sigma\right) \tag{A.10}$$

Using (33), (34), and (A.10) in (A.9), the dynamics of the sliding surface is consequently obtained as Eq. (37).

https://doi.org/10.1017/S0263574718000802 Published online by Cambridge University Press